Available online at www.sciencedirect.com
ScienceDirect
Journal of the European Ceramic Society 30 (2010) 429–434
www.elsevier.com/locate/jeurceramsoc

Optical scattering of nanocrystalline $Pb(Zr_xTi_{1-x})O_3$ films

Jarkko Puustinen [a,*], Jyrki Lappalainen [a], Jussi Hiltunen [b], Vilho Lantto [a]

[a] *Microelectronics and Materials Physics Laboratories, EMPART Research Group of Infotech Oulu, University of Oulu, Linnanmaa, FIN-90570 Oulu, Finland*
[b] *VTT Technical Research Centre of Finland, Kaitoväylä 1, FIN-90571 Oulu, Finland*

Available online 24 June 2009

Abstract

Optical characterization methods, like spectrophotometry at UV–vis-NIR wavelengths and prism-coupler method, were applied to polycrystalline $Pb(Zr_xTi_{1-x})O_3$ thin films at various thicknesses. Thin films were deposited at room temperature by pulsed laser deposition on MgO (1 0 0) substrates and post-annealed at different temperatures. X-ray diffraction and atomic force microscopy were used to characterize the crystal structure and surface morphology of the thin films, respectively.

Well oscillating transmission with a sharp fall near the absorption edge was found in films with high orientation and low surface roughness. Changes in the surface morphology and crystal orientation were found to modulate optical interference maxima and minima of the transmittance spectra and to increase the width of the TE_0 mode ($\Delta\beta \approx 0.06$) indicating an increase in the scattering losses of the films. Single-phase oriented films had sharpest coupling values ($\Delta\beta \approx 0.005$) of the TE_0 mode.

Keywords: Films; Grain size; Optical properties; PZT

1. Introduction

Ferroelectric materials, like PZT, in the form of thin films are potential candidates to be used in optical communication and signal processing applications where electrically controllable devices are needed. One of the key issues, for optical applications based on functional materials is to minimize the optical losses. For instance, to optimize the performance of the waveguide structures based on thin films, it is essential to understand the origins of the optical losses in order to minimize the scattering and absorption of the thin film structure. Optical losses of thin films have several origins, including absorption, internal scattering, and surface scattering. Absorption occurs due to defects within the grain or at grain boundaries, such as impurities and vacancies. An internal scattering losses are due to variations of the refractive index within the thin films, caused by material inhomogeneities or by grain misorientation, and surface scattering is due to surface roughness or surface waviness of the thin films.[1] The optical scattering losses by surface scattering caused by rough surface can be described by the scalar scattering theory and the transmittance losses resulted from the surface scattering can be expressed by equation:

$$T = T_0 \left\{ 1 - \exp\left[\left(-\frac{2\pi(n_1 - n_2)R_q}{\lambda} \right)^2 \right] \right\}, \quad (1)$$

where T_0, n_1, n_2, λ, R_q are total transmittance of the film, refractive index of the film and air, wavelength, and surface rms roughness, respectively, and the so called surface scattering coefficient $\alpha_{surf}(\lambda)$ can be approximately expressed as[2,3]

$$\alpha_{surf}(\lambda) = \left(\frac{2\pi(n_1 - n_2)R_q}{\lambda} \right)^2. \quad (2)$$

In this study optical scattering of polycrystalline $Pb(Zr_xTi_{1-x})O_3$ films with different crystal structure, surface morphology and small grain size are discussed.

2. Experimental

A pulsed XeCl-excimer laser (Lambda Physik COMPex 201) with wavelength of 308 nm and $Pb_{0.97}Nd_{0.02}(Zr_{0.55}Ti_{0.45})O_3$ target were used to deposit amorphous PNZT thin films with thicknesses of 50 ± 3.7 nm, 100 ± 5.6 nm, 150 ± 3.2 nm, 200 ± 10.9 nm, 300 ± 6.2 nm, 400 ± 7.3 nm, and 500 ± 13.0 nm on MgO (1 0 0) substrates. The deposition was carried out at room temperature at a base pressure of ~7 mPa. The substrate

* Corresponding author. Tel.: +358 08 5537971; fax: +358 8 553 2728.
E-mail address: jpuust@ee.oulu.fi (J. Puustinen).

0955-2219/$ – see front matter © 2009 Elsevier Ltd. All rights reserved.
doi:10.1016/j.jeurceramsoc.2009.05.047

and target were placed parallel at the distance of 35 mm. The repetition rate of the laser pulses was 5 Hz and the laser beam fluence at the target surface was 1.5 J/cm^2. After deposition, thin films were post-annealed at temperatures from 400 °C up to 1000 °C for 30 min under inverted zirconia crucible together with some PNZT powder. Both heating and cooling rates were 5 °C/min in all temperature profiles.

Crystal structure of the PNZT films was studied using X-ray diffraction (XRD) (Philips MW1380) measurements with CuKα radiation ($\lambda = 0.154$ nm). Intensities were recorded with a constant speed of 1° min^{-1} in the 2θ range 10–80°. The instrumental broadening was obtained using a large-grain polycrystalline silicon sample as standard specimen and MgO (2 0 0) substrate reflection to correct the peak position. Atomic force microscopy (AFM) (Veeco Dimension 3100) was used to study the surface morphology of the post-annealed thin films in contact mode. In order to evaluate the morphology of the thin films, bearing area curves (BAC) and the values of rms roughness R_q were calculated from AFM micrographs. Optical transmission spectra in the wavelength range from 180 nm to 3000 nm were measured using a spectrophotometer (Varian Cary 500). Refractive index n and extinction coefficient k were calculated from transmission data fitted with multiple Lorentz-oscillator model using SCI Film Spectrum software. The optical guiding properties of the polycrystalline PNZT thin films were measured using a prism-coupler (Metricon model 2010), in which laser beam with wavelength of 632.8 nm was coupled into the films using a prism pressed against thin film surface and a photodiode was used to detect the reflected light from the film. From prism-coupler measurements, the full width at half maximum (FWHM) value $\Delta\beta$ of the propagation constant β of TE_0 coupling mode was determined.

3. Results and discussion

XRD measurements showed that films post-annealed at temperatures below 500 °C were poorly crystallized and XRD patterns indicated a broad amorphous-like peak in the region of $2\theta \approx 30°$. In the post-annealing temperature range $500\,°C \leq T_{ann} < 600\,°C$, a pyrochlore phase was present in the films. Above the post-annealing temperature of 600 °C, the films had the desired perovskite structure where the trigonal phase was more preferred in films with thickness above 400 nm and in the tetragonal phase (c/a)-ratio gradually decreased as the thickness of the films increased from 50 nm to 300 nm. Same kind of thickness-dependent phase evolution has been observed also in PZT thin films having different compositions.[4,5] Strong (1 1 0) singlet peak was present in films with thicknesses above 400 nm indicating trigonal orientation and degree of a- and c-axis grain orientation of the tetragonal phase showed dependence on the post-annealing temperature so, that as the post-annealing temperature increased c-axis orientation was preferred.[6] Average grain size of the post-annealed PNZT thin films was determined using Warren–Averbach analysis for the (0 0 1) and (1 0 0) reflections of the θ–2θ XRD measurements. Only films with either trigonal or tetragonal crystal structure were included in the average grain size analysis. In Fig. 1 are shown values of the

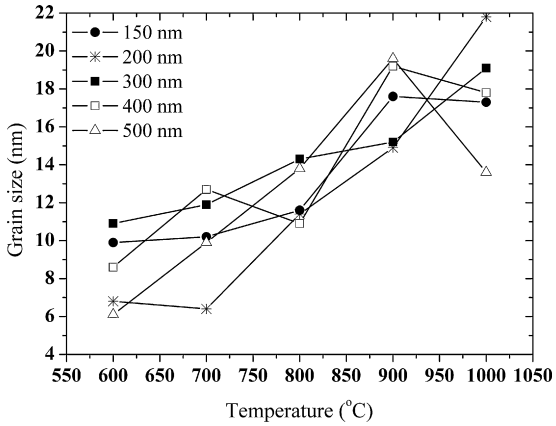

Fig. 1. Average grain size according to Warren–Averbach analysis for films with thicknesses of 150 nm, 200 nm, 300 nm, 400 nm, and 500 nm post-annealed at temperatures of 600 °C, 700 °C, 800 °C, 900 °C, and 1000 °C, respectively.

average grain size calculated according to the Warren–Averbach analysis. Average grain size of the films increased from 6 nm to 22 nm as the post-annealing temperature increased from 600 °C to 1000 °C, which corresponds quite well with previous studies.[7] It was also found that microstrain in single-phase films was usually lower as compared to films with tetragonal-trigonal phase co-existence. Same kind of correlation between the phase structure and microstrain of the films has been also observed in PNZT thin films deposited with different laser beam fluence.[8]

From AFM measurements it was found that films with amorphous structure had smooth surfaces, while in films having pyrochlore phase the surface roughness was high ($R_q > 30$ nm). For films with high tetragonal or trigonal crystal structure surface roughness were lower ($R_q \approx 10$ nm), bearing area curves steeper and surface curvatures lower compared to films with tetragonal-trigonal phase co-existence ($R_q \approx 25$ nm). Tetragonal–trigonal phase co-existence was present in films with thicknesses around 300 nm. Well defined microstructure with small grains evenly distributed throughout the films, was found in films with thicknesses 50–200 nm and 400–500 nm. Changes in the surface morphology were due to surface evolution during the post-annealing process, as previously described.[6,9]

Changes in the crystal structure and surface morphology led also to chances in the optical transmission properties of the films. In the films post-annealed at temperature of 400 °C the fall in the transmission spectra near the absorption edge was sharp in all samples. Films were transparent and, for instance, the refractive index n of a 150 nm thick film saturated at NIR wavelengths to a value $n \approx 2.40$, which is close to the value $n \approx 2.35$ of a 150 nm thick film post-annealed at temperature of 700 °C. The fall in the transmission spectra near the absorption edge of oriented single-phase films stayed sharp between post-annealing temperatures of 600–800 °C, which is typical behaviour for oriented single-phase nanocrystalline films.[10] In this temperature range films were either tetragonal (a- or c-axis oriented) or trigonal with orientation depending on the film thickness, and the grain size of the films varied between 6 nm and 14 nm. Even thought the fall near the absorption edge stayed sharp inter-

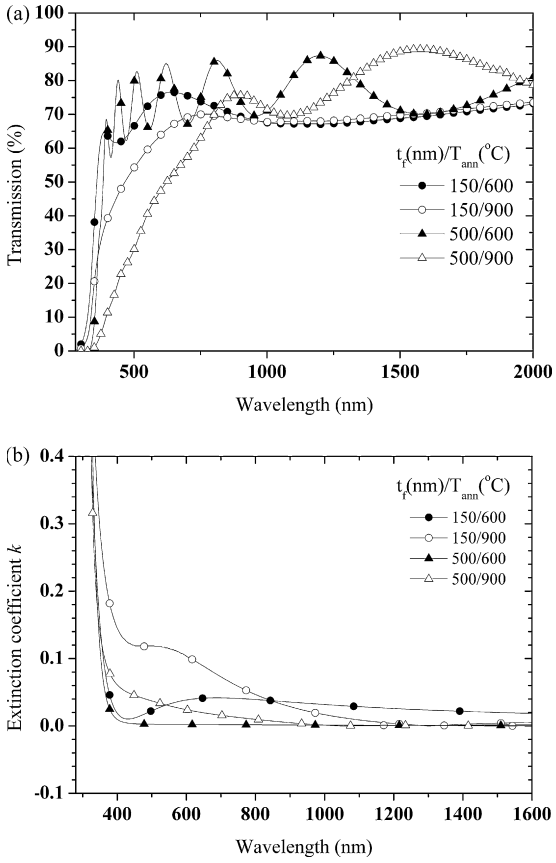

Fig. 2. (a) Transmission spectra and (b) extinction coefficients of 150 nm and 500 nm films post-annealed at temperatures of 600 °C and 900 °C.

ference maxima and minima of the transmission spectra were clearly disturbed. Suppression of oscillations in interference of transmission spectra at UV–vis wavelengths was found in every film as the post-annealing temperature increased. This indicates that some part of the light is scattered due to surface scattering leading to prolongation of the optical path for the scattered light.[11] In Fig. 2(a) and (b) are shown transmission spectra and extinction coefficients for 150 nm and 500 nm thick films post-annealed at temperatures of 600 °C and 900 °C. Transmission spectra showed very weak oscillations in interference for 150 nm and 500 nm thick films post-annealed at temperature of 900 °C. Suppression of oscillations in transmission spectra was clearly seen at UV–vis wavelengths, which was an indication of increased scattering due to changes in the surface morphology. As the optical length of the height differences due to surface roughness of the films, are comparable to the fraction of wavelength λ, oscillations in interference of transmission spectra are suppressed. By using one layer (substrate + film) multiple Lorentz-oscillator model in determining the optical parameters, suppression of oscillations in interference caused poor agreement with measured and simulated data. From Fig. 2(b) it can be seen that the extinction coefficients increased as the post-annealing temperature increased from 600 °C to 900 °C at UV–vis wavelengths. Absorption in 150 nm thick film annealed at 600 °C film started already at longer wavelengths than the absorption edge, which indicated some

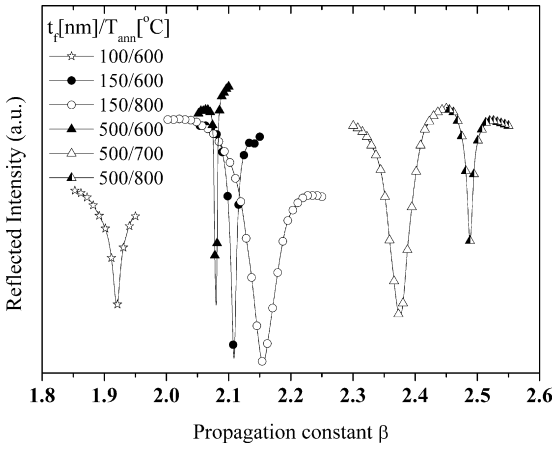

Fig. 3. TE_0 optical coupling modes for films with various thicknesses and post-annealing temperatures.

other absorption mechanism than interband absorption in the film. This might be due to absorption by localized energy states in the band gap, originating from increased disorder, defects, and grain boundary discontinuity.[12,13] According to our previous studies porosity of PLD deposited PNZT thin films is negligible.[14–16] Transmission at the wavelength of $\lambda = 633$ nm decreased from 76.5% to 66.2%, and extinction coefficient increased from 4.1×10^{-2} to 9.4×10^{-2} for films with thickness of 150 nm as the post-annealing temperature increased from 600 °C to 900 °C. Correspondingly for 500 nm thick films, transmission at the wavelength of $\lambda = 633$ nm decreased from 83% to 51% and extinction coefficient increased from 2.1×10^{-3} to 2.1×10^{-2} as the post-annealing temperature increased from 600 °C to 900 °C. Due to increased suppression of oscillations in interference, which led to poor agreement of measured and simulated data, multiple Lorentz-oscillator model gave exaggerated k values for films post-annealed at temperature of 900 °C.

Optical guiding properties of the PNZT thin films were analyzed using the prism-coupler method. In this method light with a wavelength of $\lambda = 632.8$ nm is guided into the film through one side of the prism, which is pressed against the film surface, and reflected light from the film is detected with photodiode, which is placed on the other side of the prism. Reflectivity dips at a certain value of the propagation constant β corresponding to excitation of coupling modes, which are called m lines, representing the guiding mode order. Characteristics of the guiding mode spectrum include that the number of guiding modes increases with thickness, all exited modes propagates with their unique propagation constant, and full widths at half maximum ($\Delta\beta$) of the guiding modes are sensitive to microstructure of the thin films. Both transverse electric (TE) and transverse magnetic (TM) waves can be exited depending on the crystal properties of the thin films.[17–19] In Fig. 3 there are TE_0 guiding modes for a film with thickness of 100 nm post-annealed at a temperature of 600 °C, 150 nm thick films post-annealed at 600 °C and 800 °C, and 500 nm films post-annealed at temperatures of 600 °C, 700 °C, and 800 °C, respectively, showing light coupling in the polycrystalline PNZT thin films. Samples

were fully crystallized into the perovskite phase, either trigonal or tetragonal depending on the film thickness. From Fig. 3 it can be seen that the propagation constant β of 150 nm and 500 nm thick films increased as the post-annealing temperature increased from 600 °C to 800 °C and from 600 °C, 700 °C to 800 °C, respectively, which indicated an increase in the refractive index of the films. Increase in the refractive index may be due to an increase in the average grain size of the film and also in the degree of grain orientation, which is similar to the case of a previous study with PNZT thin films.[7] As the heat-treatment temperature increased from 600 °C to 800 °C, 150 nm thick films changed their orientation from tetragonal *a*-axis to tetragonal *c*-axis orientation and the average grain size increased from 9.9 nm to 11.6 nm. For 500 nm thick films trigonal orientation was profoundly present and grain size increased from 6.1 nm to 13.8 nm as the post-annealing temperature increased from 600 °C to 800 °C. Full widths at half maximum $\Delta\beta$ of the TE_0 guiding modes for films in Fig. 3 were 0.0144, 0.0123, 0.0631, 0.0048, 0.0189, and 0.0114, respectively, and corresponding R_q values were 3.7 nm, 7.3 nm, 17.1 nm, 6.9 nm, 13.4 nm and 11.2 nm, respectively. Full widths at half maximum $\Delta\beta$ values of the guiding modes were determined by fitting the measured data using Lorentz function. Notice that the increase in the $\Delta\beta$ values of 150 nm and 500 nm thick films in Fig. 3 follow the changes in the corresponding R_q values. Similar correlation between R_q values and TE_0 mode widths was also found in rf-sputtered $LiNbO_3$ films.[19] Sharpest $\Delta\beta$ value was found for film with thickness of 500 nm post-annealed at temperature of 600 °C ($\Delta\beta = 0.0048$), which is close to $\Delta\beta$ value of epitaxial $BaTiO_3$ ($\Delta\beta = 0.0011$).[6] For films with high surface roughness ($R_q > 20$ nm) it was not possible to guide light to the film due to large surface scattering. Although TE_0 guiding mode was used for the mode-width analysis, losses increased rapidly in the higher order modes.[18] This was clearly observed in films with thicknesses of 300 nm and 400 nm. $\Delta\beta$ values of TE_1 optical guiding modes for 300 nm and 400 nm thick films post-annealed at temperatures of 700 °C and 900 °C were 0.1740 and 0.1030, respectively. Interference maxima and minima were clearly suppressed in the UV–vis wavelength range of the transmission spectrum of 300 nm thick film post-annealed at 700 °C, and the losses can be attributed to the tetragonal–trigonal phase coexistence, which led to an increase in the surface waviness and R_q values ($R_q \approx 25$ nm), causing an enhanced light scattering from the surface of the films. Further increase in the surface waviness and surface roughness in 300 nm thick film post-annealed at 800 °C totally blocked mode coupling. In Fig. 4(a) and (b) are shown surface rms roughnesses together with surface scattering coefficients and in Fig. 5(a) and (b) are shown surface scattering coefficients together with TE_0 mode widths for films with thicknesses of 150 nm and 500 nm post-annealed at different temperatures. Scattering coefficients were calculated using Eq. (2) at wavelength $\lambda = 632.8$ nm. From Fig. 4(a) and (b) it can be seen that surface scattering coefficients increased as the surface roughness increased, which is a clear indication of a changes in surface morphology. This result is similar to optical scattering studies reported on niobium oxide films.[3] Values of surface scattering coefficients of 150 nm thick films were low up

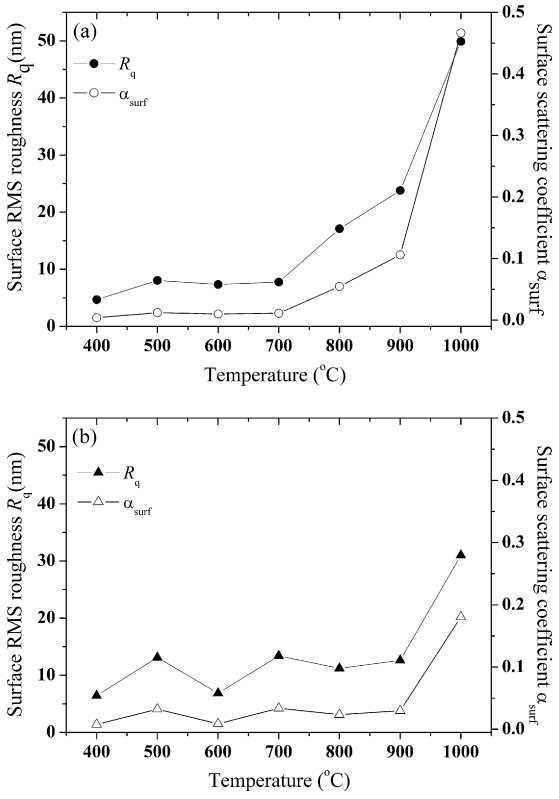

Fig. 4. Surface RMS roughness (R_q) and surface scattering coefficients (α_{surf}) values of (a) 150 nm and (b) 500 nm thick films post-annealed at temperatures of 400–1000 °C.

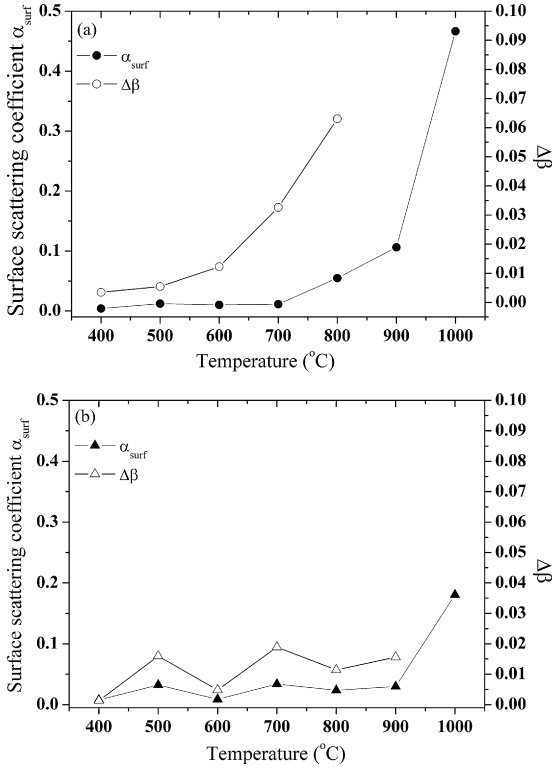

Fig. 5. Surface scattering coefficients (α_{surf}) and $\Delta\beta$ values of films with thicknesses of (a) 150 nm and (b) 500 nm post-annealed at temperatures of 400–1000 °C.

to post-annealing temperature of 700 °C. As the post-annealing temperature increased to 800 °C, values of α_{surf} increased due to secondary grain growth process.[9] Broadening of the TE_0 modes of 150 nm and 500 nm thick films follows quite well the scattering coefficient values, as seen in Fig. 5(a) and (b). TE_0 mode width increased for 150 nm thick films from 0.0123 to 0.0631, and the surface roughness increased from 7.4 nm to 17.1 nm, as the post-annealing temperature increased from 600 °C to 800 °C. Effect of the secondary grain growth process is seen in Fig. 5(a) as an increase in $\Delta\beta$ value of 150 nm thick film at post-annealing temperature of 800 °C. Smaller changes in the $\Delta\beta$ values were found in 500 nm thick films as compared to those in 150 nm thick films, which can be seen by comparing Fig. 5(a) and (b). This was due to well defined microstructure of the 500 nm thick films up to the post-annealing temperature of 900 °C, which led to small α_{surf} values. TE_0 mode width of 500 nm thick films increased from 0.0048 to 0.0156, and the surface roughness increased from 6.9 nm to 12.6 nm, as the post-annealing temperature increased from 600 °C to 900 °C, showing good light guiding properties up to post-annealing temperature of 900 °C.

By combining results shown in Figs. 1 and 5(a) and (b) it is clearly seen that surface scattering dominates the optical scattering process. Average grain sizes of films with different thicknesses increased from 6 nm to 22 nm with increasing post-annealing temperature, which were negligible small compared to the optical wavelengths used in the experiments. With decreasing grain size the volume ratio of grain boundaries increases extensively, and thus the grain boundary scattering should dominate the optical properties. However, in Fig. 5(b) it is shown that propagation constant $\Delta\beta$ of the films post-annealed at low temperatures with small grain sizes and high grain boundary contribution, is small. Smaller FWHM values ($\Delta\beta$) of the propagation constant β means higher coupling efficiency of the optical power in to the waveguiding film and smaller scattering. So the increase in $\Delta\beta$ values was mainly due to changes in the surface morphology of films leading to an increase in the surface scattering.

4. Conclusions

Crystal structure, average grain size, surface morphology and optical properties of pulsed laser deposited $Pb(Zr_xTi_{1-x})O_3$ thin films on MgO (1 0 0) substrates with thicknesses of 50 nm, 100 nm, 200 nm, 300 nm, 400 nm, and 500 nm and post-annealed at various temperatures were studied using X-ray diffraction, atomic force microscopy, spectrophotometry, and prism-coupler method. Tetragonal distortion was found to decrease as the thickness of the films increased from 50 nm to 300 nm, showing that trigonal orientation was more preferred in films with thicknesses above 400 nm. Good optical transmission and guiding properties were found in films with single-phase orientation, small grain size, and low surface roughness and, thus, low surface scattering coefficient. Changes in the surface morphology and crystal orientation were found to modulate oscillations in the interference pattern and to modulate the full width at half maximum ($\Delta\beta$) values of TE_0 optical guiding mode indicating strong dependence on the surface scattering process. Sharpest optical coupling width, $\Delta\beta \approx 0.0048$, was found in the film with thickness of 500 nm post-annealed at 600 °C, while highest value, $\Delta\beta \approx 0.0631$, was found in film with thickness of 150 nm post-annealed at 800 °C.

Acknowledgements

Author acknowledges Foundation of Tauno Tönning for financial support. Part of this research was carried out in Micro and Nanotechnology Center (MNT) of University of Oulu.

References

1. Fork, D. K., Armani-Leplingard, F. and Kingston, J. J., Optical losses in ferroelectric oxide thin films: is there light at the end of the tunnel? *Mater. Res. Soc. Symp. Proc.*, 1995, **361**, 155–166.
2. Poruba, A., Fejfar, A., Remes, Z., Springer, J., Vanecek, M., Kocka, J., Meier, J., Torres, P. and Shah, A., Optical absorption and light scattering in microcrystalline silicon thin films and solar cells. *J. Appl. Phys.*, 2000, **88**(1), 148–160.
3. Lai, F., Li, M., Wang, H., Hu, H., Wang, X., Hou, J. G., Song, Y. and Jiang, Y., Optical scattering characteristic of annealed niobium oxide films. *Thin Solid Films*, 2005, **488**, 314–320.
4. Kelman, M. B., Schloss, L. F., McIntyre, P. C., Hendrix, B. C., Bilodeau, S. M. and Roeder, J. F., Thickness-dependent phase evolution of polycrystalline $Pb(Zr_{0.35}Ti_{0.65})O_3$ thin films. *Appl. Phys. Lett.*, 2002, **80**(7), 1258–2179.
5. Kelman, M. B., McIntyre, P. C., Hendrix, B. C., Bilodeau, S. M. and Roeder, J. F., Structural analysis of coexisting tetragonal and rhombohedral phases in polycrystalline $Pb(Zr_{0.35}Ti_{0.65})O_3$ thin films. *J. Mater. Res.*, 2003, **18**(1), 173–179.
6. Puustinen, J., Lappalainen, J. and Lantto, V., Variations of optical properties with phase co-existence in nanocrystalline PZT thin films. *Ferroelectrics*, 2008, **370**(1), 46–56.
7. Lappalainen, J., Hiltunen, J. and Lantto, V., Characterization of optical properties of nanocrystalline doped PZT thin films. *J. Eur. Ceram. Soc.*, 2005, **25**, 2273–2276.
8. Lappalainen, J., Frantti, J., Hiltunen, J., Lantto, V. and Kakihana, M., Stress and film thickness effects on the optical properties of ferroelectric $Pb(Zr_xTi_{1-x})O_3$. *Ferroelectrics*, 2006, **335**, 149–158.
9. Puustinen, J., Lappalainen, J. and Lantto, V., Effect of microstructure and surface morphology evolution on optical properties of Nd-modified $Pb(Zr_xTi_{1-x})O_3$ thin films. *Thin Solid Films*, 2008, **516**, 6458–6463.
10. Ganguly, A., Mandal, S. K., Chaudhuri, S. and Pal, A. K., Electrical and optical properties of $ZnS_{0.05}Se_{0.95}$ nanocrystalline thin films. *J. Appl. Phys.*, 2001, **90**(11), 5652–5660.
11. Poruba, A., Fejfar, A., Salyk, O., Vanecek, M. and Kocka, J., Surface and bulk light scattering in microcrystalline silicon for solar cells. *J. Non-Cryst. Solids*, 2000, **271**, 152–156.
12. Srikant, V. and Clarke, D. R., Optical absorption edge of ZnO thin films: the effect of substrate. *J. Appl. Phys.*, 1997, **81**(9), 6357–6364.
13. Gaidi, M., Amassian, A., Chaker, M., Kulishov, M. and Martinu, L., Pulsed laser deposition of PLZT films: structural and optical characterization. *Appl. Surf. Sci.*, 2004, **226**, 347–354.
14. Lappalainen, J., Frantti, J. and Lantto, V., Electrical and mechanical properties of ferroelectric thin films laser ablated from $Pb_{0.97}Nd_{0.02}(Zr_{0.55}Ti_{0.45})O_3$ target. *J. Appl. Phys.*, 1997, **82**(7), 3469–3477.
15. Lappalainen, J., Ivanov, S. A. and Lantto, V., Secondary grain growth and surface morphology of post-annealed nanocrystalline $Pb_{0.97}Nd_{0.02}(Zr_{0.55}Ti_{0.45})O_3$ thin films. *J. Appl. Phys.*, 2002, **92**(10), 6153–6159.
16. Tuominen, J., Lappalainen, J., Hiltunen, J., Ollila, J. and Lantto, V., Piezoelectric thin-film unimorph actuator for optical fibre alignment applications. *J. Opt. A: Pure Appl. Opt.*, 2006, **8**, 398–404.

17. Ulrich, R. and Tonge, R., Measurement of the thin film parameters with a prism coupler. *Appl. Opt.*, 1973, **12**(12), 2901–2908.
18. Tien, P. K., Light waves in thin films and integrated optics. *Appl. Opt.*, 1971, **10**(11), 2395–2413.
19. Dogheche, E., Lansiaux, X. and Remiens, D., *m*-Line spectroscopy for optical analysis of thick $LiNbO_3$ layers grown on sapphire substrates by radio-frequency multistep sputtering. *J. Appl. Phys.*, 2003, **93**(3), 1165–1168.